Simultaneous Retrieval of Surface Roughness Parameters for Bare Soils from Combined Active-Passive Microwave SMAP Observations

Anke Fluhrer, *Member, IEEE*, Thomas Jagdhuber, *Senior Member, IEEE*, Ruzbeh Akbar, *Member, IEEE*, Peggy O'Neill, *Fellow, IEEE*, Dara Entekhabi, *Fellow, IEEE*

Abstract— An active-passive microwave retrieval algorithm for simultaneous determination of soil surface roughness parameters (vertical RMS height (s) and horizontal correlation length (l) is presented for bare soils. The algorithm is based on active-passive microwave covariation including the improved Integral Equation Method (I2EM) and is tested with global SMAP observations. Estimated retrieval results for s and l are overall consistent with values in the literature, indicating the validity of the proposed algorithm. Sensitivity analyses showed that the developed roughness retrieval algorithm is independent of permittivity for $\varepsilon_s > 10$ [-]. Furthermore, the physical model basis of this approach (I²EM) allows application of different autocorrelation functions (ACF), such as Gaussian and exponential ACFs. Global roughness retrieval results confirm bare areas in deserts such as Sahara or Gobi. However, the type of ACF used within roughness parameter estimation is important. Retrieval results for the Gaussian ACF describe a rougher surface than retrieval results for the exponential ACF. No correlations were found between roughness results and the amount of precipitation or the soil texture, which could be due to the coarse spatial resolution of the SMAP data. The extension of this approach to vegetated soils is planned as an add-on study.

Index Terms— correlation length, 1²EM, radar, radiometer, RMS height, SMAP

I. INTRODUCTION

A. Motivation for surface roughness estimation

The estimation and monitoring of geophysical parameters via earth-observation satellites is crucial for improving our understanding of global environmental and hydrological processes. Soil roughness is an essential parameter in physical processes related to water, energy, and nutrient flow and exchange, since it characterizes the boundary between the pedosphere and atmosphere [1]. Soil roughness influences microwave signals from soil surfaces and contributes to measurements from active as well as passive sensors. Both radar backscatter $|S_{PP}|^2$ [dB] and microwave emissivity E_P [-], based on brightness temperature TB_P [K], are sensitive to surface roughness [2], [3].

Despite its importance for environmental applications, soil roughness has played a minor role in land parameter retrieval with microwave remote sensing in recent decades [4], [5]. For instance, soil roughness is an important parameter in land surface modeling of soil erosion applications, because it defines the soil surfaces that

Manuscript received; revised; accepted. Date of publication. (Corresponding author: Anke Fluhrer.)

This work was supported in part by the MIT-Germany Seed Fund "Global Water Cycle and Environmental Monitoring using Active and Passive Satellite-based Microwave Instruments."

- A. Fluhrer and T. Jagdhuber are with the German Aerospace Center, Microwaves and Radar Institute, Muenchener Strasse 20, 82234 Weßling, Germany (e-mail: Anke.Fluhrer@dlr.de). A. Fluhrer is with the University of Augsburg, Institute of Geography, Alter Postweg 118, 86159 Augsburg.
- R. Akbar and D. Entekhabi are with the Department of Civil and Environmental Engineering, Massachusetts Institute of Technology, Cambridge, MA 02139 USA.
- P. E. O'Neill is with the NASA Goddard Space Flight Center, Greenbelt, MD 20771 USA.

represent "the interface between the eroding soil body and the erosive agent" [6], [1], [3], [5].

Retrieval of geophysical parameters such as soil roughness or soil moisture is mainly performed at lower frequencies, like at L-band (1.4 GHz), due to the higher sensitivity of active and passive microwave signatures to soil moisture (under vegetation) compared to C-band (~ 6 GHz) and higher frequency bands [3], [7], [8]. Further, the operational monitoring of soil moisture content on global scales has been mainly performed continuously with passive microwave sensors up to now. Passive microwave sensors are used predominantly since soil roughness and vegetation hold a stronger influence on backscatter than on soil-emitted brightness temperature [9].

The primary disadvantage of passive-only retrievals is the coarse spatial resolution of microwave radiometers (> 40 km), which is sufficient for large-scale applications, such as global climate modelling. Yet, for weather forecasting and agricultural yield management, soil moisture information of at least 10 km spatial resolution is desired [10]. Active microwave sensors provide a higher spatial resolution than passive microwave sensors. Unfortunately, studies in recent years have shown that estimations of geophysical parameters, more precisely soil moisture, on the basis of radar-only retrievals are more prone to errors than radiometer-only or combined methods [9]. This might be due to two reasons: Firstly, there are difficulties in quantifying all occurring scattering effects [9], [11-13], and secondly, the impact of terrain and vegetation morphology are often not considered adequately in radar retrievals due to complex plant structures [9]. Thus, the combination of both active and passive sensor systems can improve monitoring of geophysical parameters, such as soil surface roughness, by leveraging the advantages of both sensors while overcoming their individual limitations.

Currently, the existing soil moisture retrieval algorithms for a joint processing of radar and radiometer microwave satellite data are neural network based approaches [e.g. 14, 15], the change detection method [7], [16], [17], [18], and the Soil Moisture Active Passive (SMAP) optional [10] and the SMAP baseline [10], [19] downscaling algorithms. In all of these algorithms soil roughness is considered only as a secondary effect. For one, soil roughness is corrected either by collecting multi-configuration data (variety of frequency and/or polarization) or by optimizing it within the parameter retrieval algorithm until the model predictions coincided with the actual measured data. Second, roughness is considered as static and fixed to a constant value for single land cover classes according to the classification of the International Geosphere-Biosphere Program (IGBP), as done within the SMAP L2 & L3 soil moisture algorithms [20]. However, Saatchi et al. noted that for a precise monitoring of soil moisture, accurate determination of surface roughness is key to correctly deriving soil moisture information from radar data [21].

B. Parameterization of Surface Roughness in Remote Sensing

The two fundamental parameters describing soil surface roughness are the standard deviation of the surface height variation (or vertical RMS height), with its related autocorrelation function (ACF), and the horizontal correlation length [8]. The degree of correlation between two laterally separated locations of one surface can be estimated through the surface correlation function $p(\xi)$, with ξ as displacement

between those two locations. With increasing separation between two locations on the surface, $p(\xi)$ decreases, and at a certain distance, the so-called horizontal correlation length, the vertical RMS heights at the two locations are considered statistically uncorrelated [8].

Due to the non-standardized naming convention, the terminology for both parameters is ambiguous. Common parameterizations for the vertical RMS height are S_D , σ or s [4], [8], [22], [23], and for the horizontal correlation length L_C or l [2], [24]. In this study, the standard deviation of the surface height variation is denoted by s [cm], with its related ACF [-], and the horizontal correlation length by l [cm], which is the naming convention already used, e.g., in [1], [8], [25], [26].

For the sake of completeness, it should be mentioned that passive microwave retrievals often refer to a different roughness parameter. They are using a radiative transfer model to simulate effects of surface roughness on measured brightness temperature TB_P [4]. This model is the analytical zero-order solution to the Radiative Transfer equation, commonly referred to as the tau-omega $(\tau - \omega)$ model [27], which is basis for numerous microwave emission models, such as the L-band Microwave Emission of the Biosphere (L-MEB) model, employed in the current SMOS L2 algorithm [23]. Within these models, soil emission is calculated based on a semi-empirical approach first proposed by Wang & Choudhury 1981 [28], known as HQN [24] or H-Q model [29]. Wang & Choudhury [28] pointed out that the Fresnel equations can be used to describe the reflectivity of a smooth but not a rough soil surface. In the latter case, scattering of the incident wave occurs in many directions and the reflected parts "in the specular direction would be lower than the Fresnel reflectivity" [28]. To consider reflectivity losses caused by increasing surface roughness, the soil roughness loss factor, $h = H_R \cdot cos^N \theta$, was introduced [4]. Here, another roughness parameter, called H_R [23], is used to characterize roughness effects on passive microwave signatures.

In this study, we determine the vertical RMS height and the horizontal correlation length of a surface, and can link h with s by $H_R = (2 \cdot s \cdot k)^2$, where k [cm⁻¹] is the wave number $(k = 2\pi/\lambda)$ [4], [22], [23], [30]. In the HQN model, the parameter Q is called the polarization mixing factor which accounts for differences in values between the horizontal and the vertical polarization. Lastly, within the HQN model to describe the reflectivity of a rough surface, the parameter N accounts for multi-angular and dual-polarization measurements which is set equal to two in most studies [24], [28].

In addition to s and l, a third roughness parameter is defined as the root-mean-square (RMS) slope m, "a quantity proportional to the ratio of [s to l]" [8], indicating the degree of roughness of one surface. For a one-dimensional height profile for one random surface, m is defined as $m = [-s^2p''(0)]^{1/2}$, with p''(0) as the second derivative of the surface correlation function $p(\xi)$, evaluated at the origin ($\xi = 0$). Since $p(\xi)$ is an even function, p''(0) is a negative quantity [8]. For modeling of electromagnetic scattering at soil surfaces, assumptions of the functional forms of $p(\xi)$ have to be made. The most common forms are the exponential and the Gaussian correlation functions. In case of a Gaussian ACF, m can be calculated by $m = \sqrt{2} s/l$ [8], [31]. In theory, in case of an exponential ACF a surface does not have a RMS slope. This is due to the fact, that this correlation function is not differentiable at the origin, since in order to describe a correlation it has to be an even function [32]. Hence, Dierking, 2000 presented the derivation of an "effective" RMS slope for exponentially correlated surfaces, which always has to be considered in relation to the frequency of the acquisition system. Therefore, the exponential RMS slope can be calculated by m = $\sqrt{2/\pi} * s/l * \sqrt{5kl - arctan(5kl)}$ [31]. The RMS slope m is one of the validation criteria for the Small Perturbation Model (SPM) [8]. In general, for L-band, m should be lower than 0.3 [8] or 0.4 [31], [32] in case of bare soil surfaces with moderate RMS heights [32].

Overall, the type of employed wave scattering model is essential for modelling of electromagnetic wave interaction with vegetation or soil and should be considered carefully depending on its advantages and disadvantages.

When observing soil surfaces with remote sensing techniques, the observed roughness scales are mainly a function of the wavelength of the sensing system. In detail, the observable roughness scales can either be equivalent or larger (but limited by resolution cell extent) than the wavelength of the sensing system, whereas smaller scales would not contribute significantly to the signal [8]. In the field of microwave remote sensing, surface roughness is mainly observed at centimeter scale, since "[a]t microwave frequencies, the wavelength is on the order of centimeters to a few tens of centimeters" [8]. Exceptions are found for surfaces that include effects of large-scale topography when resolution cell sizes are in the order of the topographic variations.

The objective of this study is to simultaneously determine the vertical (s) and horizontal (l) components of bare soil surface roughness through the combination of active and passive microwave data on global scale.

II. Data

Data for this study come from the NASA SMAP mission [3]. This mission was launched in 2015 with the aim to exploit synergies between active and passive instruments at L-band frequency. It is the first soil moisture dedicated space-borne mission developed to provide moisture products from active and passive microwave satellite data [3], [33]. Unfortunately, the SMAP radar went out of service in July 2015 after only three months of operations, but the SMAP radiometer continues to deliver high-quality data [34]. Due to the radar failure, the investigation period with SMAP data in this study is limited to the period from 14th of April until 7th of July 2015.

The data used in this study are the SMAP L1B Radar Half-Orbit Time-Ordered low resolution backscatter $|S_{PP}|^2$ [35], the SMAP L1C Radiometer Half-Orbit Time-Ordered Brightness Temperatures TB_P [36], the physical soil temperature T_S and soil moisture obtained from the SMAP L3SM_P products [37], all posted on a 36 km Equal-Area Scalable Earth-2 (EASE-2) grid [20], [38].

In order to guarantee analyses exclusively over bare soils we filter the global surface roughness results for vegetation, water or snow. We used the vegetation optical depth (VOD) posted on a 36 km EASE-2 grid from the SMAP dataset processed with the multitemporal dual-channel retrieval algorithm (MT-DCA) [38], and the surface condition quality flags for snow and frozen ground from the SMAP L3 Radiometer Global and Northern Hemisphere Daily 36 km EASE-Grid Freeze/Thaw State [39] for filtering. Pixels with VOD greater than 0.06, with more than one day covered by snow or frozen ground during the investigation period, or with more than 5% water fraction are masked out.

Previous studies emphasized the impact of large-scale roughness effects due to topography on satellite microwave observations [e.g. 40, 41]. Therefore, significant topography is normally excluded or treated with special care in satellite data products of various missions such as SMOS [42] or SMAP [33]. In this study, effects of topography on 36 km-scale SMAP observation-based soil roughness estimates are assumed to be non-significant mainly due to two reasons: First, after filtering of SMAP retrieval input parameters (backscatter, emissivity) only regions with DEM (digital elevation model) slope angles, extracted from the SRTM V4 [43], smaller than 25° are analyzed. Hence, only bare soils with flat to moderate terrain are considered. Second, at the resolution cell size of 36 km intra-cell variations in DEM slope angles are assumed to compensate themselves (co-occurrence of up- and down-slopes) up to a certain degree. This might be reflected in non-significant correlations (R=0.42 for s & R=-0.32 for l) between SMAP retrieval results and

the standard deviation of DEM slopes within the 36 km resolution cells.

III. METHODS

In the course of developing combined active-passive microwave retrieval algorithms for geo-physical parameters (e.g. soil moisture), the relationship between the radar backscatter ($|S_{PP}|^2$) and the emissivity ($E_P = T_{b_P}/T$) of a radiometer was found to be quasi linear [20]. For the SMAP algorithms, it is expressed by the two regression parameters α and β , with α_{P-PP} [-] being the P-polarized intercept and β_{P-PP} [-] being the P-polarized slope of the linear regression (1) [20], [44].

$$E_P = \alpha_{P-PP} + \beta_{P-PP} * |S_{PP}|^2$$
 (1)

For bare soils, the intercept α_{P-PP} is 1, due to the fact that vegetation cover is absent [45]. Therefore, the slope β_{P-PP} describes the covariation between emissivity and backscatter for bare soils and is defined as follows [44]:

$$\beta_{P-PP} = \frac{E_P - 1}{|S_{PP}|^2} = \frac{\frac{T_{DP}}{T_S} - 1}{|S_{PP}|^2},\tag{2}$$

where T_S is the surface physical temperature within the top 5 cm of the soil [2].

In (2) β_{P-PP} is referred to as the covariation parameter, for respective polarization P. The specific form of (2) allows us to calculate β_{P-PP} based on electromagnetic interaction models of bare surface backscatter and emissivity, β_{P-PP}^{Model} [-], like the SPM, the Integral Enhanced Method (I²EM) or the Numerical Maxwell Model in 3-D (NMM3D), ordered with increasing model complexity.

 β_{P-PP} can also be calculated from quasi-simultaneously acquired active and passive microwave measurements, henceforth β_{P-PP}^{Data} . The only limiting factor is that both sensors (radar and radiometer) must have the same spatial resolution in order to observe roughness at the same scales.

For surface roughness estimation, we calculate β_{P-PP}^{Model} and β_{P-PP}^{Data} based on simulated and data-based backscatter and emissivity, respectively. Then, we minimize the absolute difference between model prediction β_{P-PP}^{Model} and the calculated observations-driven β_{P-PP}^{Data} for s and l estimation by selecting the β_{P-PP}^{Model} based on the permittivity closest to the actual permittivity of the SMAP L3SM_P product (cf. sec. II.) (converted according to the dielectric mixing model of Topp et al. [46]).

In order to avoid invalid combinations of surface roughness parameters, we use the RMS slope m with m < 0.4 to filter the retrieval results (cf. sec. I.B.). As mentioned before, this condition is also used as validity criterion for the SPM [8], which is equivalently valid for I²EM when L-band frequency is applied [47]. The details for modelled and data-based covariation parameters are as follows.

A. Model-based Retrieval of Active-Passive Microwave Covariation

 β_{P-PP}^{Model} is calculated by forward simulations of surface emissivity (E_P) and backscatter $(|S_{PP}|^2)$ using (2). We first defined a physically meaningful and sufficiently large range of values for $s \in [0, 10]$ cm in 0.1 cm steps, and $l \in [1, 40]$ cm in 0.5 cm steps. The third input parameter is soil permittivity and ranges from $\varepsilon_s \in [2.6, 78]$ in 0.1 steps. Within forward wave scattering models several types of ACFs for simulations can be assumed. It is a requirement for simulating the surface backscatter and emissivity and is detached from *in situ* or remote sensing data. In this study, results for s and l are calculated using either Gaussian or Exponential ACF.

In this study, we simulate backscatter and emissivity values with the I²EM to calculate β_{P-PP}^{Model} [8]. The reason for employing the I²EM is its common physical basis for backscatter and emissivity based on s and l, frequency f, type of ACF, incident angle θ and soil

permittivity ε_s [8], [47], [48]. Details on model formulations (computer codes) can be found in the supplement of [8]. Because of its analytical formulation, I²EM is preferred over computationally more expensive numerical methods, such as the NMM3D [49].

B. Data-based Retrieval of Active-Passive Microwave Covariation

The covariation parameter calculated with (2) based on microwave observations is called data-based covariation parameter β_{P-PP}^{Data} [-]. This parameter is dependent on the observation conditions and the sensitivity of the recording system to the natural phenomenon.

In this study, β_{P-PP}^{Data} , is calculated based on SMAP observations specified in section II.

C. Advantage of Active and Passive Microwave Signature Combination

As an example of how the joint use of radar and radiometer can improve soil moisture estimations, Fig. 1 shows overlays of radaronly and radiometer-only cost functions along permittivity ε_s and roughness parameter s simulated with the I²EM.

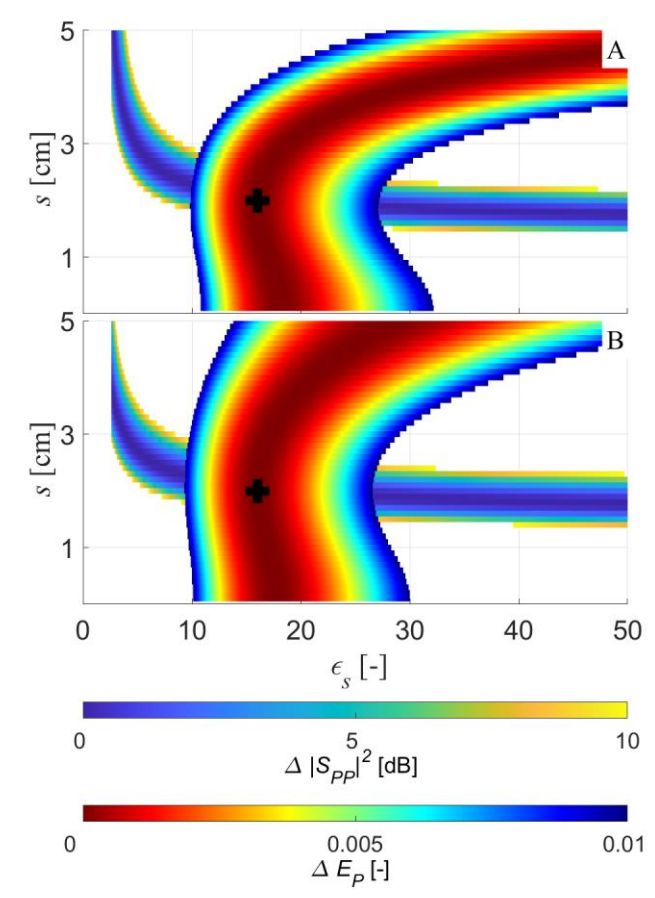


Fig. 1. Overlay of radar-only ($\Delta |S_{PP}|^2 = ||S_{PP}|^2(\bar{x}) - |S_{PP}|^2_{True}|^2$ [dB]) and radiometer-only ($\Delta E_P = |E_P(\bar{x}) - E_{PTrue}|^2$ [-]) cost functions modelled with l²EM assuming a Gaussian ACF: (A) Overlay for horizontal polarization, (B) Overlay for vertical polarization. The black cross is the true test point (global minimum) at input parameters $\varepsilon_s = 15$ [-], s = 2 cm and l = 14 cm. Study similar to Akbar et al, 2017 [34].

Similar to Akbar *et al.* the computed backscatter $\Delta |S_{PP}|^2$ (radaronly) and emissivity ΔE_P (radiometer-only) spaces are displayed for a vector of unknowns ($\bar{\mathbf{x}} = [\varepsilon_s, s, l]$) [34]. ε_s ranges from 2.6 to 50 in 0.1 steps, s values from 0.05 cm to 10 cm, and l values from 1 cm to 21 cm, each in 0.1 cm steps. In Fig. 1, we assume l = 14 cm and plot $\Delta |S_{PP}|^2 < -30$ dB and $\Delta E_P < 0.01$ [-] to emphasize model predictions in the vicinity of the true test point (black cross), which is

the global minimum of the cost function. The results for the horizontal polarization (cf. Fig. 1A) and the vertical polarization (cf. Fig. 1B) are shown individually since "scattering polarization behaviors are different" [34].

It can be understood from Fig. 1 that the possible range of valid permittivity values that yield $\Delta |S_{PP}|^2 \cong 0$ extend over the entire range of initial ε_s values. This holds true for both polarizations. The possible range of values for s spans from 1.2 cm to 5 cm. In the case of the radiometer, the possible range of permittivity values is slightly reduced and extends from 14 to 50 for the horizontal polarization (cf. Fig. 1A) and from 14 to 30 for the vertical polarization (cf. Fig. 1B). However, the range of possible values for s now covers the entire range of initial s values (from 0.05 cm to 5 cm). Therefore, if only radars or radiometers are used, it is not clear which pairs (ε_s , s) lead to most accurate estimates. This disadvantage is further amplified by the presence of measurement noise.

By combining radar- and radiometer-only cost functions, the search space for optimum parameter values is significantly reduced, since the complementary physics of backscatter and emissivity limits the possible parameter search space. Consequently, lower retrieval errors can be achieved compared to retrievals only based on one sensor. The combined approach effectively reduces the susceptibility of radars to permittivity and the susceptibility of radiometers to roughness.

IV. SENSITIVITY ANALYZES

A. Simulation-based performance assessment of the retrieval algorithm

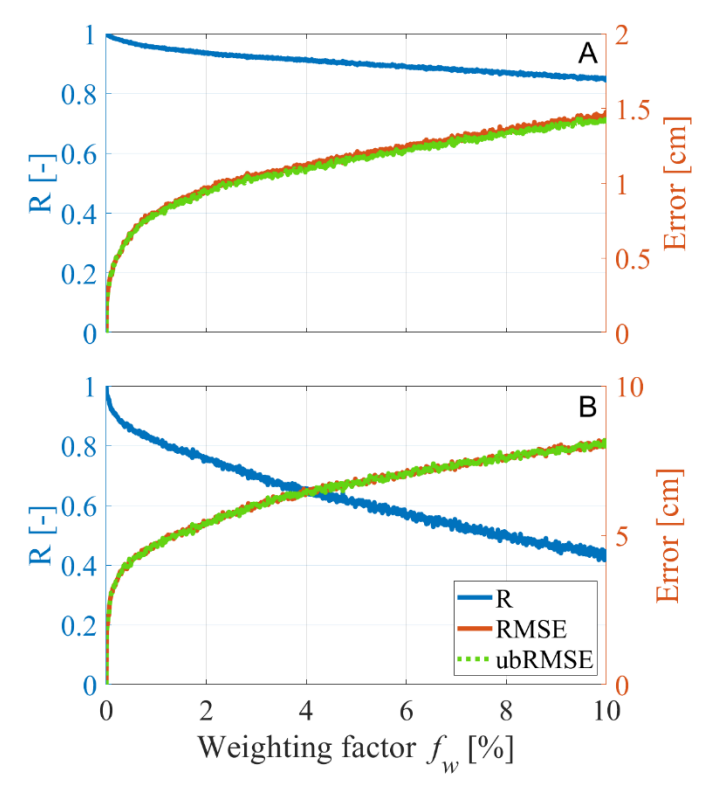


Fig. 2. Comparison of correlation coefficient (R), root-mean square error (RMSE), and unbiased root-mean square error (ubRMSE) between original roughness parameters \mathbf{s} and \mathbf{l} and perturbated roughness parameters $\mathbf{\hat{s}}$ and $\mathbf{\hat{l}}$ from retrieval input parameters with added random noise, along the weighting factor \mathbf{f}_w controlling the strength of added random noise ranging from 0% to 10%. (A) Vertical RMS-height (\mathbf{s} , $\mathbf{\hat{s}}$). (B) Horizontal correlation length (\mathbf{l} , $\mathbf{\hat{l}}$).

In order to assess the performance of the proposed active-passive covariation based retrieval algorithm for surface roughness parameter

estimation, simulations with noise-added retrieval input parameters have been performed. We simulated backscatter coefficients and emissivity values with the I2EM for a wide range of roughness and permittivity values, based on which we estimated the surface roughness parameter s and l with the proposed approach. Afterwards, we added random noise to the I²EM simulated backscatter and emissivity. The subsequently estimated surface roughness parameters based on the noise-added simulations are denoted by \hat{s} and \hat{l} . The random noise is generated based on the variance of the respective simulated parameter (backscatter, emissivity), randomly generated values uniformly distributed in the interval [0, 1], and a weighting factor f_w for each realization between 0% and 10%. In total, 1001 realizations are incorporated. The results for \hat{s} and \hat{l} are then compared to the originally estimated roughness parameters s and l. Fig. 2 displays the correlation coefficient (R), root-mean square error (RMSE) and unbiased root-mean square error (ubRMSE) between original and perturbated surface roughness estimates as a function of the weighting factor f_w (strength of added noise).

It can be seen that correlation coefficients decrease to 0.85 between s and \hat{s} and to 0.43 between l and \hat{l} for the maximum f_w of 10%. Here, the decrease for surface parameter l is more rapid and larger in magnitude than for surface parameter s, showing that l is more sensitive to added noise on input parameters (backscatter, emissivity). The RMSE and ubRMSE increase concurrently with increasing f_w from 0 to 1.42 cm for s and from 0 to 7.98 cm for l. In summary, this simulation study serves as a first-order performance assessment of the proposed retrieval approach. However, validation of the approach with real world observations is paramount in a follow-on study.

B. Analysis of sensitivity on soil permittivity

As shown in Fig. 1 in an overlay study, the influence on backscatter and emissivity is twofold with roughness and permittivity of the soil. In order to minimize the influence of permittivity, the covariation formulation in (2) (cf. sec. III.) was developed in this study. As (2) represents a ratio, it is anticipated that the permittivity-dependent reflectivity term in the emissivity and backscatter formulation (cf. [44] for modelling details) is comparable and minimizes its influence.

In order to evaluate this permittivity influence on our proposed covariation-based retrieval algorithm, we compared the full range of physically reasonable ε_s -values with the estimated model-based covariation parameter β_{P-PP}^{Model} , computed with NMM3D as well as I²EM (cf. sec. III.A.). As shown in Fig. 3, β_{P-PP}^{Model} remains nearly constant over the entire range of permittivity values for both employed models except for small permittivity values. β_{P-PP}^{Model} changes only for ε_s lower than approx. ten, representing arid and hyper-arid soils. The reason for this is found in the formulation of covariation with emission over backscatter (cf. (2), sec. III.). The backscatter falls exponentially to very low values for these small permittivity values, which in turn causes larger dynamics in covariation. However, for $\varepsilon_s > 10~\beta_{P-PP}^{Model}$, calculated based on backscatter and emissivity from I²EM, is insensitive to permittivity dynamics. Consequently, both model simulations (NMM3D & I²EM) predict that the retrieval algorithm is independent of permittivity variations in case of non-arid soils.

As the independence of our approach for $\varepsilon_s > 10$ is only based on NMM3D and I²EM simulations, the exact permittivity value from which on our approach is insensitive may vary with other models, depending on the respective model design.

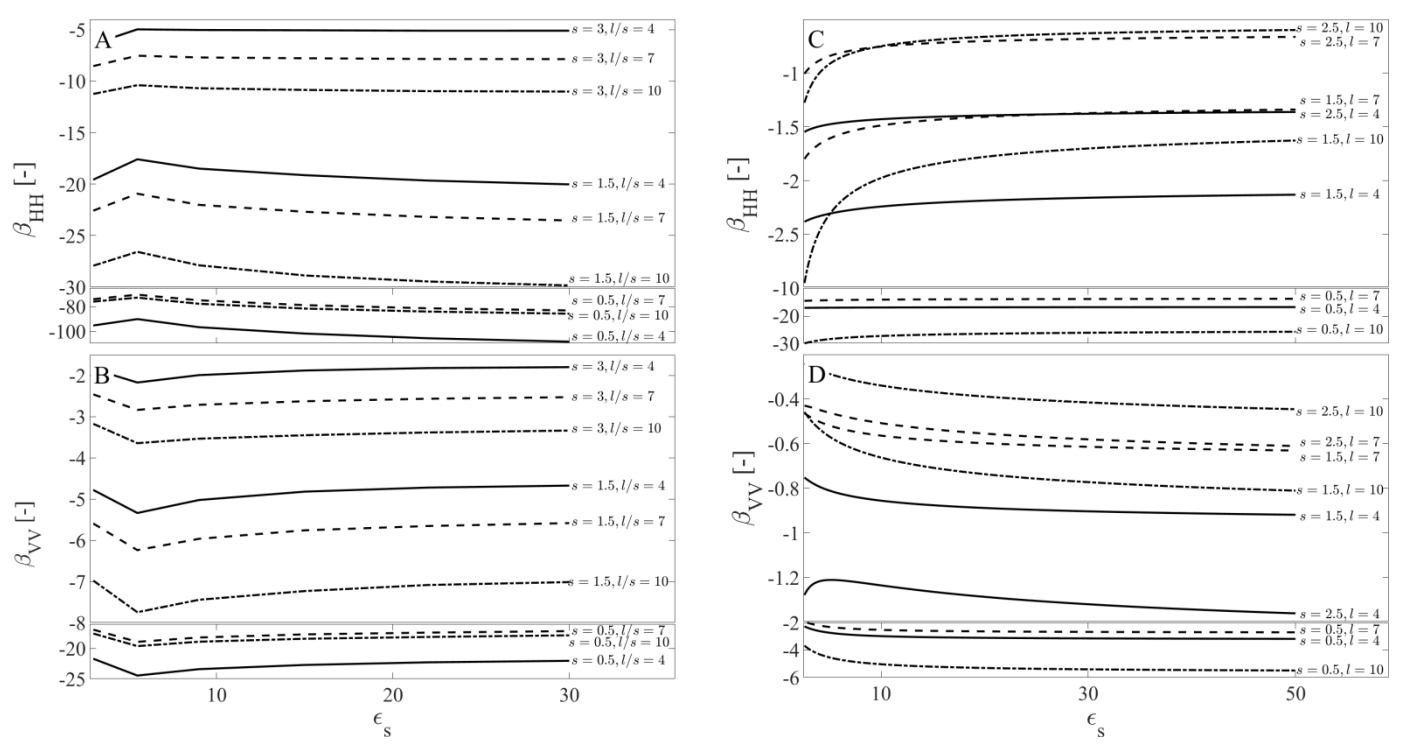


Fig. 3. Influence of soil permittivity ε_s on covariation parameter β_{P-P}^{Model} modelled with NMM3D or 1²EM assuming a Gaussian ACF, s of 0.5 cm, 1.5 cm and 3 cm and the ratio l/s of 4 cm, 7 cm and 10 cm. (A) NMM3D results for β_{H-HH}^{Model} , (B) NMM3D results for β_{V-VV}^{Model} , (C) 1²EM results for β_{H-HH}^{Model} , (D) 1²EM results for β_{V-VV}^{Model} . The y-axes are interrupted since β_{P-P}^{Model} increases to large negative values for very smooth surfaces.

V. RESULTS

This section presents the roughness results obtained from SMAP observations using the proposed covariation-based active-passive algorithm (cf. (2), sec. III.). Additionally, the results for varying ACFs are compared and analyzed in the context of changing weather and soil conditions.

A. Results of Surface Roughness Parameter Estimation

In the following, the retrieval results for the roughness parameters s and l are presented. Note that the proposed approach only applies to bare surfaces. These regions are located almost exclusively in North Africa, Asia or Australia. For reasons of better readability, we will therefore only display results for this sub-region.

Fig. 4 illustrates the median of estimated s and l for the sub-region Africa-Asia-Australia, which were calculated assuming a Gaussian ACF. The results for s are between 0.35 cm and 7 cm, with a majority of the values (\sim 72.3%) between 0.35 cm and 2.5 cm. The lowest values for s are found within the Sahara, and the highest values at the edges of deserts (e.g. Sahara, Gobi) or in the Arabian Peninsula due to increasing vegetation cover (e.g. shrublands) or rocks (cf. Fig. 4A). The results for l range between 1.75 cm and 20.5 cm, with correlation lengths mostly (\sim 86.4%) of 6 cm to 16 cm. The lowest values for l are estimated, for example, in the Sahara or in the southern part of Australia. The highest values for l are found in the northwestern part of Australia as well as in Kazakhstan and Mongolia (cf. Fig. 4B).

Comparing the roughness estimates calculated assuming either a Gaussian (cf. Fig. 4) or an exponential ACF (cf. Fig. 5), the roughness patterns for the two ACFs generally appear similar. However, results for the Gaussian ACF are higher for s and lower for l compared to the results for the exponential ACF. About 72.3% of all s values assuming a Gaussian ACF are between 0.35 cm and 2.5 cm, whereas over 82.2% of all s values are located in the same range when assuming an exponential ACF. In addition, over 86.4% of

values for l are located between 6 cm to 16 cm for the Gaussian ACF, but only 60.2% are located in that same range for the exponential ACF, since overall larger l values are retrieved (cf. Fig. 5).

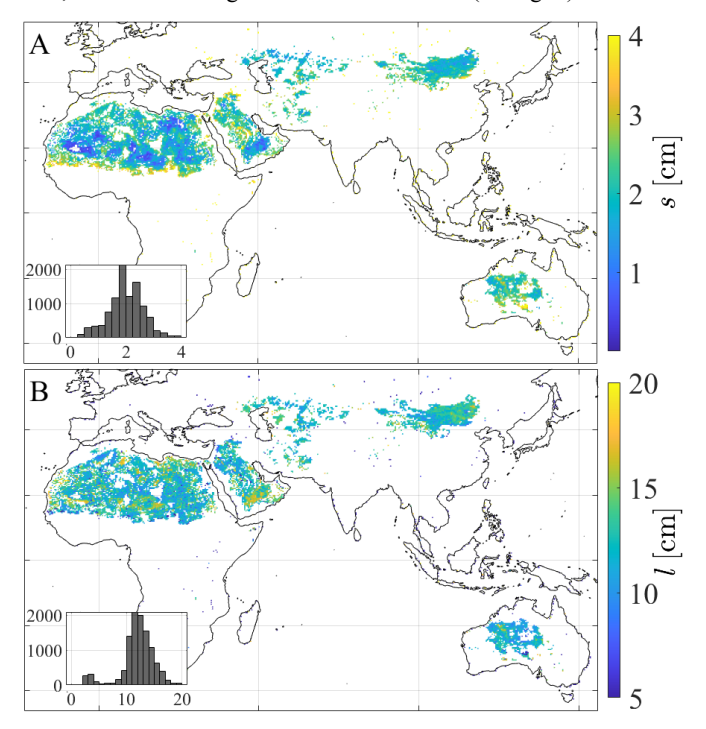


Fig. 4. Temporal median (April-July 2015) of estimated surface roughness parameters s and l from SMAP observations for the sub-region Africa-Asia-Australia assuming a Gaussian ACF. (A) Vertical RMS height s, (B) Horizontal correlation length l.

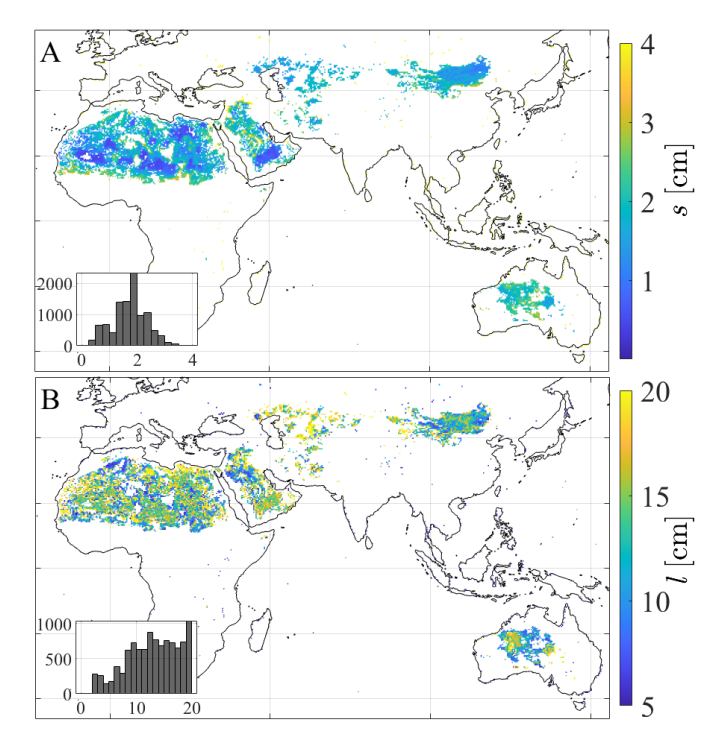


Fig. 5. Temporal median (April-July 2015) of estimated surface roughness parameters s and l from SMAP observations for the sub-region Africa-Asia-Australia assuming an exponential ACF. (A) Vertical RMS height s, (B) Horizontal correlation length l.

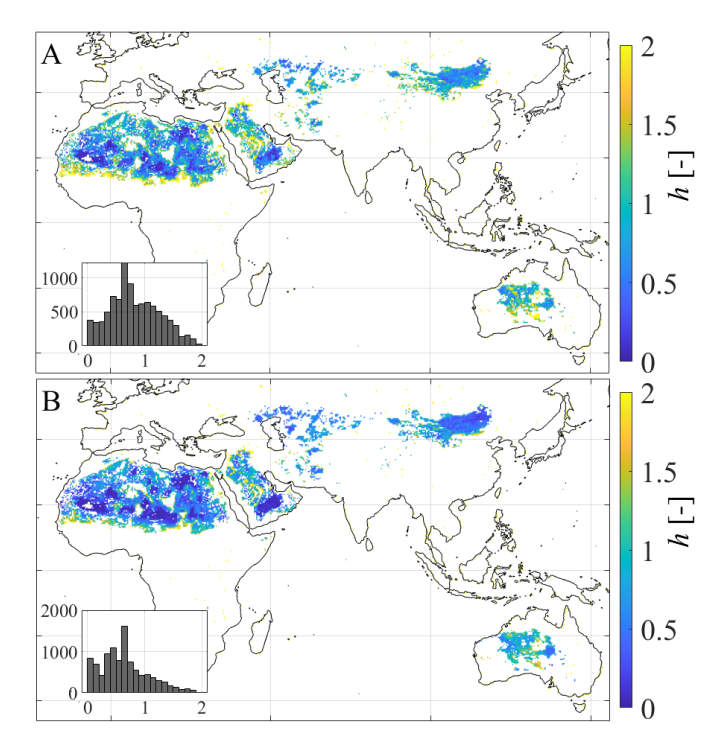


Fig. 6. Temporal median (April-July 2015) of estimated roughness loss factor h for the sub-region Africa-Asia-Australia based on surface roughness parameters s from SMAP observations. (A) Gaussian ACF, (B) Exponential ACF.

Based on estimated roughness results for s and with N=2 (cf. sec. I.B.), the roughness loss factor h is calculated assuming a Gaussian ACF (cf. Fig. 6A) or an exponential ACF (cf. Fig. 6B). The values for h are in the range between 0 and 2. As can be seen in Fig. 6, assuming a Gaussian ACF, the majority of values (\sim 79.7%) are

located between 0 and 1.5 with a peak between 0.6 and 0.7 (cf. inset of Fig. 6A). In case of an exponential ACF, approx. 86.1% of all values for h are located in the range between 0 and 1.5. However, its peak is also between 0.6 and 0.7, whereas the magnitude is dropping significantly towards higher values. Hence, overall lower values for h are obtained assuming an exponential instead of a Gaussian ACF. By definition, the spatial patterns of h are equivalent to the ones of h (cf. Fig. 4-6).

For a more detailed investigation of the differences between the results of both ACFs, we analyzed their power spectra, as described in [50]. Defined as "a measure of the amplitude of each Fourier component scattered by a rough surface" [51], the power spectrum explains the surface type assumed for the ACF. We calculated the respective power spectrum for both ACFs along different wave numbers according to [50] and normalized them by their respective amplitude to allow direct comparisons.

Fig. 7 shows the normalized power spectra of both ACFs and the case for L-band ($\lambda = 21$ cm) as a red dashed line. The roughness values calculated with an exponential ACF stay below the level of the values calculated with Gaussian ACF. Hence, the Gaussian ACF describes a rougher soil surface, whereas the exponential ACF describes a smoother soil surface at L-band, according to presented retrieval results displayed in Fig. 4 and 5.

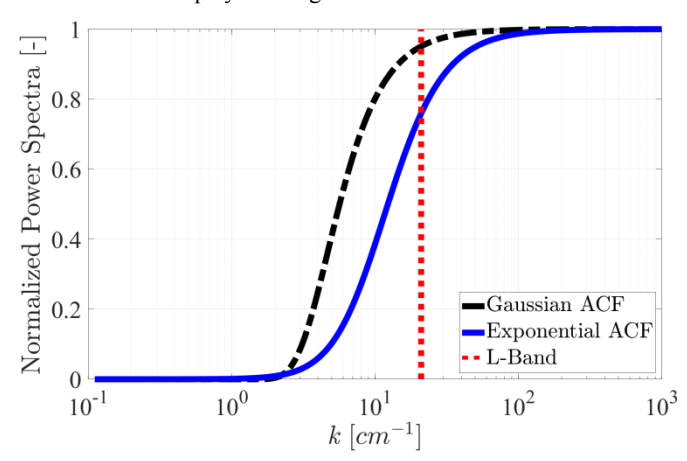


Fig. 7. Comparison of the normalized power spectra [-] for the Gaussian (black line) and exponential (blue dashdot line) autocorrelation functions (ACF) at L-band (red dashed line) along wave number k [cm⁻¹], calculated based on (9) and (10) of [50].

B. Comparison of Surface Roughness Estimates with Precipitation and Soil Conditions

Analyses are performed to investigate possible correlations between estimated roughness parameters and external factors such as weather or soil conditions, since precipitation or wind as well as specific soil textures potentially influence soil surface roughness.

For temporal analyzes, we used data from the Yanco Agricultural Institute, Bureau of Meteorology, Australia [52] to investigate the influence of precipitation on soil surface roughness with time.

In Fig. 8 we compare the daily *in situ* precipitation measurements and the corresponding SMAP soil moisture [37] values with roughness retrieval results at the Yanco test site, Australia.

For one, the variations in surface roughness parameters across the entire period from 14^{th} of April until 7^{th} of July 2015 show differences between lowest and highest estimate of 2 cm for s and 10 cm for l, assuming a Gaussian ACF, as well as differences of 0.75 cm for s and 8 cm for l, assuming an exponential ACF. Hence, estimated roughness parameters s and l vary less during the investigated period if an exponential ACF is assumed.

Second, it can be seen that soil moisture and precipitation follow each other and correlate, as expected. However, both show no correlation with the SMAP-based results for s and l, regardless the

type of ACF (cf. Fig. 8). This lack of correlation between roughness results and precipitation was also tested between roughness and soil moisture for the entire sub-region Africa-Asia-Australia (not shown here). Analysis of temporal correlation between the change of estimated roughness parameters s and l and the SMAP soil moisture dynamics show no significant correlation, whereby the most frequent value in the analyzed histograms is zero with a standard deviation of 0.14.

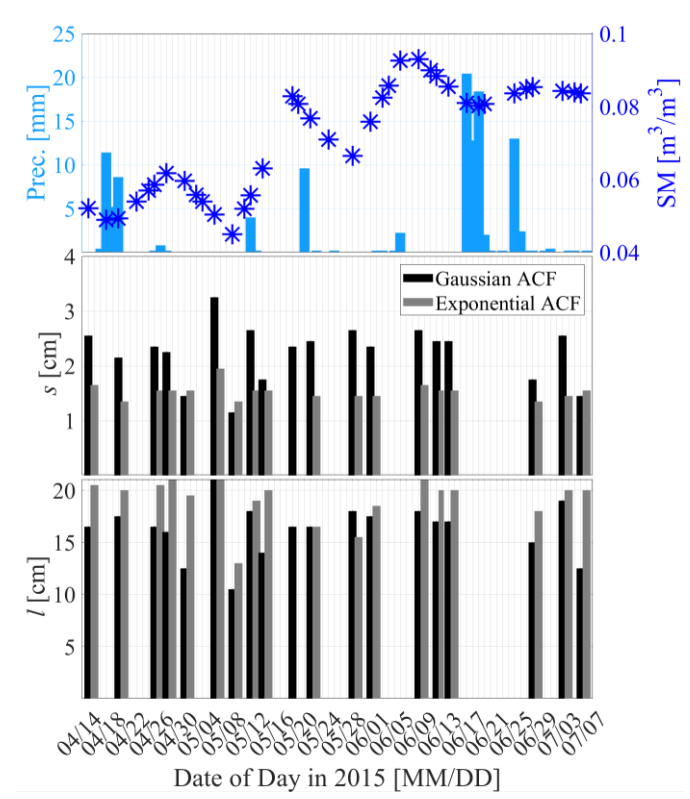


Fig. 8. Daily precipitation measurements from the Yanco agricultural institute, Bureau of Meteorology, Australia [52] (bright blue bars) and soil moisture from SMAP [37] (dark blue stars) in comparison with retrieval results for surface roughness parameters s and l, based on SMAP observations, assuming a Gaussian ACF (black bars) or exponential ACF (gray bars), at the Yanco weather station (NSW, 34.60°S, 146.42°E).

In addition, the estimated roughness patterns were compared with VOD from SMAP MT-DCA retrievals [38] and sand or clay fractions of soils from [53], both posted on the 36 km EASE-2 grid.

Fig. 9 shows that retrieval results for s are slightly increasing until VOD class 0.015 to 0.03 and then slightly decrease. In contrast, results for l are slightly decreasing until VOD class 0.015 to 0.03 and then slightly increase. Despite the overall similar distribution patterns, the value ranges for both ACFs are significantly different for roughness parameter l, with much larger ranges for the exponential ACF. However, no influence of vegetation could be observed at higher VOD values. In extended analyses up to VOD of 1.12 (not shown here), we get higher values for s and lower values for s and lower values for s and s and s and s and vegetation. The value ranges of estimated s and s for all VOD classes from 0 to 0.06 thus confirm the effective filtering before estimating the surface roughness parameters (cf. Section II.).

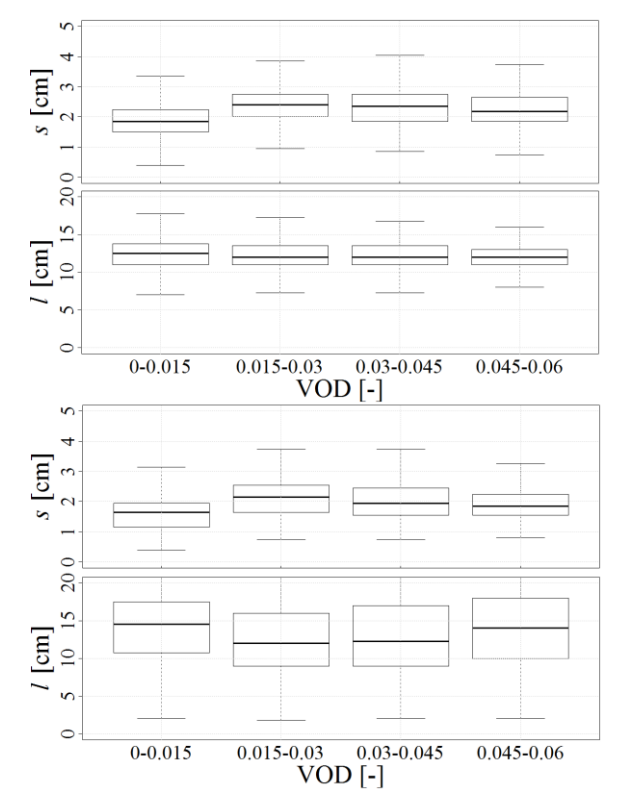


Fig. 9. Comparison of estimated surface roughness parameters *s* and *l* with vegetation optical depth (VOD) [-] [38], both from SMAP observations for the sub-region Africa-Asia-Australia. (A) Gaussian ACF, (B) Exponential ACF.

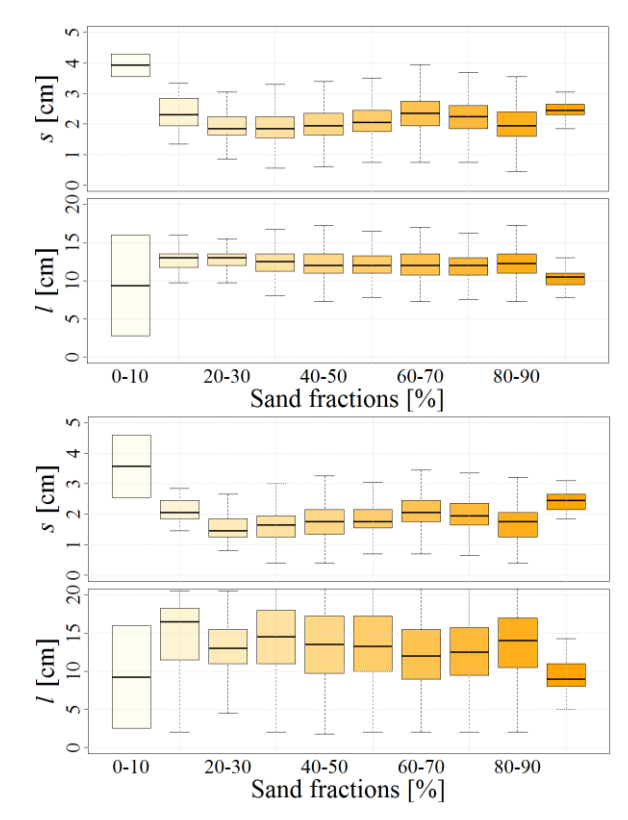


Fig. 10. Comparison of estimated surface roughness parameters s and l retrieved from SMAP observations with sand fractions from [53] for the subregion Africa-Asia-Australia. (A) Gaussian ACF, (B) Exponential ACF.

Lastly, we compared surface roughness results with the sand and clay fractions used as ancillary data within the SMAP parameter

retrievals [53], in order to analyze if soil texture might influence the roughness retrieval of a soil surface. Fig. 10 shows that the overall distribution patterns are quite similar for both employed ACFs. Similar to results displayed in Fig. 9, the value ranges are larger for the exponential ACF than for the Gaussian ACF. It can be seen that estimated s peaks for the smallest sand fraction (0-10%). On the contrary, results for estimated l are lowest for the smallest sand fraction. Additionally, the overall dynamic of l along increasing sand fractions (from 20% to 90%) is very low with absolute differences in median values of only 0.75 cm (Gaussian ACF), and 2.5 cm (exponential ACF) (cf. Fig. 10). In summary, the value ranges for s are similar for both ACFs, whereas the ranges for l assuming an exponential ACF are approximately two to three times larger than for the Gaussian ACF. However, the variation between sand fractions is reasonable and does not show a distinct correlation between roughness parameters and sand fractions.

When comparing the roughness results with clay fractions (not shown here), the most significant finding is that there is no correlation between clay fractions and the soil surface roughness parameters, similar to the case for sand fractions. Another finding is that there are no estimates of s and l for clay fractions greater than 70%. The fact that no roughness results overlap with clay fractions greater than 70% is consistent with the global distribution of clay fractions from the Harmonized World Soil Database (HWSD) [54].

VI. DISCUSSION

Our covariation-based approach requires equivalent spatial resolution for radar and radiometer acquisitions in order to observe roughness at the same scales. Most space-borne radar sensors provide a much higher resolution than radiometer sensors. In the case of the SMAP mission, the radar had a spatial resolution of ~3 km until its failure, whereas the radiometer has a resolution of ~40 km [3]. In this study we used the SMAP low resolution radar and radiometer data with the same spatial resolution of 36 km. Since our approach is limited to simultaneously acquired polarimetric active/passive microwave datasets with comparable spatial resolutions, data suitable beyond this study include the airborne PALS datasets [16], [55] or the space-borne AQUARIUS data [56]. Despite these limitations in acquisition and resolution, our roughness retrieval technique outperforms ground-based sensing methods in terms of acquisition time and spatial coverage.

For evaluation of the proposed approach, we conducted several model-based sensitivity studies, compared retrieval results with literature values, and investigated possible correlations of roughness parameters with precipitation or soil texture. These analyzes will be discussed in the following. A direct validation based on experimental surface roughness data is not feasible due to the lack of available (in situ) datasets at satellite foot print scale (36 km).

The covariation-based approach including the forward model I^2EM for the retrieval of s and l provides the possibility of employing varying ACFs and the simultaneous estimation of both roughness components with centimeter precision. Although we are only able to retrieve a wavelength-dependent roughness scales (here L-band), this approach enables the simultaneous estimation of both surface roughness parameters s and l by minimizing the influence of soil moisture (cf. sec. IV). The study from [47] showed that the l^2EM is in good agreement with the SPM at low frequencies and with the standard Kirchhoff model (KM) at high frequency regions.

For SPM the roughness influence on backscatter and emissivity is a multiplicative factor to the reflection coefficient, detailed in [44]. Hence, forming the ratio in (2) (cf. sec. III.) should cancel the permittivity influence, if reflection coefficients in backscatter (Bragg scattering) and emission (Fresnel scattering) are identical. This is the case for horizontal polarization, but not for vertical polarization [44]. Thus, a residual dependence on soil moisture remains, which we analyzed in Section IV.B. These analyzes showed that this

dependence is strongest for low permittivity and approaches towards a constant value for higher permittivity. In detail, for permittivity values of ten and higher the value of the SPM-based ratio of Bragg to Fresnel scattering coefficients is approaching to a constant value of six. Therefore, a quasi-independence from soil permittivity for values of ten and higher is found when estimating roughness parameters which motivates the combined active-passive microwave approach. Similar to SPM, analyses presented in this study based on I^2EM delineated that our covariation-based approach is independent of permittivity for values $\varepsilon_S > 10$ (cf. sec. IV.B.).

However, in this study we are only presenting results for the subregion Africa-Asia-Australia since our approach is limited to bare soils. These regions are mostly arid to hyper-arid with very low permittivity which hardly changes in space and time due to the lack of precipitation. Hence, the approach presented in this study minimizes the permittivity-dependency in two ways. On the one hand, our covariation-based approach is independent of permittivity for non-arid soils ($\varepsilon_s > 10$) by utilizing the covariation formulation (cf. sec. III., (2)). On the other hand, our presented roughness retrievals (cf. sec. V.) are quasi-independent of permittivity since we are only analyzing bare soils of dry regions with almost static soil moisture content. We tested this in a small add-on study where we fixed the input permittivity for all bare soil areas to a constant value of three and retrieved s and l. Analyses showed that we achieved very similar results as with inserting SMAP-based permittivity, with average RMSE for the entire sub-region Africa-Asia-Australia of 0.33 cm (s) or 0.87 cm (l) assuming a Gaussian ACF.

Within the proposed approach, we consider the two commonly applied ACFs of Gaussian and exponential type for characterization of the soil surface. Previous studies by [25] and [45] showed that for rather smooth bare surfaces the correlation function is close to the exponential ACF, whereas for very rough surfaces it is close to the Gaussian ACF. Especially for surface roughness of agriculturally managed soils, parameterization is more complex and variable, since the ACF is affected by the characteristics of tillage, spanning several roughness scales. Nonetheless, also for agriculturally managed soils most studies confirm an exponential ACF for smooth and Gaussian ACF for very rough surfaces (e.g. after plowing) [25], [57], [58]. Moreover, previous studies pointed out that surface roughness parameters are close to an exponential ACF when sensing over bare soils at L-Band [11], [29], [59]. Comparison of roughness results outlined the differences between both ACFs. We estimated values for s mainly in the range between 0.35 cm and 2.5 cm and for l between 6 cm to 16 cm, assuming a Gaussian ACF. For the assumption of an exponential ACF we estimated overall lower s and higher l values. Thus, the exponential ACF describes a smoother roughness pattern whereas the Gaussian ACF describes a rather rough surface roughness pattern, equivalent to literature [25], [57], [58]. Ogilvy and Foster [51] investigated in a numerical study Gaussian and exponential correlation functions of theoretically generated random rough surfaces. They found that the exponential ACF tends to correlate roughness on a fine scale due to a rapid loss of correlation. By contrast, the Gaussian ACF decreases more slowly over distance and hence tends to correlate roughness not on a very fine scale [51]. Their explanation for varying roughness correlations was found to be the shape of the respective power spectra. In the case of the exponential ACF, it is a Lorentzian transform of the correlation function, whereas in the case of the Gaussian ACF it is given by the Fourier transform of the correlation function [51]. Hence, the influence of the employed ACF type is distinct and the assumption of Zhixiong et al. that for homogeneous agricultural fields the ACF is unrelated to surface roughness conditions cannot be confirmed here [60].

In this study, we also presented results for the roughness loss factor h, which is the prominent parameter used in passive microwave retrievals based on the HQN-model [24], [28] (cf. sec. I.B.). Results

for h are located mainly between 0 and 1.5 with most values between 0.6 and 0.7, independent of the employed type of ACF. In the literature, typical values for H_R are located between 0 and 1.7, depending on the type and amount of vegetation canopy [24]. These correspond to h values between 0 and 1 (cf. sec. I.B.). Values for H_R greater than 1 are only estimated for forests, with typical values for grass or open shrublands mostly around 0.4 [24], which equals an h value of 0.23.

With our covariation-based approach, where h peaks between 0.6 and 0.7, we are apparently overestimating h since our study areas are limited to bare soils only. Nonetheless, similar studies which are estimating the single scattering albedo ω directly instead within the $\tau - \omega$ model are also retrieving higher values compared to theoretical definitions [61]. Hence, we directly retrieve s and subsequently h, with estimated roughness values for h fitting to the expected smooth to moderately rough bare surfaces.

For detailed analyses of temporal changes within estimated surface roughness parameters and possible correlations with precipitation we investigated results at the Yanko station, Australia. Surface roughness changes with weather (e.g. precipitation, wind) and agricultural managing techniques (e.g. plowing) [1]. Hence, we correlated retrieved s and l parameters with respective precipitation measurements over the entire investigation period (April to July 2015) but could not find significant correlations. Although, consequential "meteorological impacts cause a smoothing of the soil surface" [1] no such influence of rain events on estimated roughness parameters could be detected in this study. Reason for this is most likely related to the coarse spatial resolution of the SMAP data, since the impacts of rainfall events are limited to the respective affected surface. Also the study from [62] showed that precipitation can lead to changes in surface roughness, but these changes strongly dependent on the initial condition of the soil surface. Further, the assumption maybe only applies to agricultural managed soils right after tilling, when the soil surface is disturbed. Zhao et al., points to various studies regarding soil surface roughness variation due to different tillage practices and water erosion processes [62].

Surface roughness results and analyzes based on small-scale experimental microwave data from NASA's APEX12 campaign can be found in [63].

For detailed analyses of globally retrieved roughness patterns from SMAP observations, we compared results for s and l with sand or clay fractions. From those analyses, it can be understood that for our study setup the respective sand or clay fraction of a soil shows no distinct influence on s and l. However, we compared all roughness results retrieved from SMAP observations at once. This means that we do not consider different types of soils. Thus, comparisons of roughness results with individual major soil types to account for sand or clay dominated soils is needed to investigate the relation between surface roughness and specific soil types in more detail [64].

VII. SUMMARY AND CONCLUSIONS

This study presents a covariation-based active-passive microwave retrieval algorithm for simultaneous estimation of vertical and horizontal soil surface roughness components (s, l) from bare soils. Within this approach we use radar and radiometer data from both horizontal and vertical polarizations with equivalent spatial resolution to calculate the active-passive microwave covariation for each individual radar-radiometer acquisition pair (no time series needed). This way, the approach enables a simultaneous retrieval of both roughness parameters (s, l) over a larger area (compared to *in situ* measurements).

Results show that the proposed approach leads to valid retrievals of s and l, with consistencies of more than 90% between model simulations and roughness results.

By conducting a series of model-based (NMM3D & I^2EM) sensitivity tests, it was found that the influence of permittivity (soil moisture) on our covariation-based approach is only significant for (hyper-) arid soils with $\epsilon_s < 10$ (cf. sec. IV). But for these soils the permittivity is small and static along space and time, which enables fixing its value to a constant. First tests (not shown) for the subregion Africa-Asia-Australia affirm this option.

We also tested the effectiveness of our filtering of data, in order to ensure analyses exclusively over bare soils, based on VOD values. Since no influence of vegetation could be observed at higher VOD values we concluded that the filtering prior to the estimation of roughness results for vegetation was successful.

Moreover, no significant correlation between precipitation and surface roughness parameters could be found despite the often applied assumption that soil surface roughness smoothens with precipitation. One reason could be that this assumption only applies to agricultural managed soils after tilling. Furthermore, results outline that changes in surface roughness are not correlated to changes in soil moisture.

Similar to correlations between estimated roughness patterns and precipitation or soil moisture, no correlation could be found between roughness parameters and sand or clay fractions. The reason for the lack of correlations in all correlation analyses might be that we investigate global roughness patterns from SMAP observations with ~36 km spatial resolution where precipitation effects might be non-dominant in the recorded signal.

Detailed investigations regarding the influence of the assumed type of ACF revealed that both Gaussian and exponential ACF describe different types of roughness patterns, and our conclusions are consistent with previous studies. Hence, the employed type of ACF for surface roughness estimation is crucial and must be considered carefully.

In summary, the retrieved roughness parameters have the potential to improve soil moisture estimates, even from satellite data and for global scales. This supports soil moisture estimation for hydrometeorology or climate research.

The proposed technique for surface roughness retrieval from combined active and passive microwave signatures is currently limited to bare soils. In order to enable the estimation under vegetated soils, our covariation-based algorithm needs to be updated for vegetation-based scattering as well as emission [44].

ACKNOWLEDGMENTS

The authors would like to thank Mark Luetzner from DLR for the English proofreading. The authors are grateful to MIT for supporting this research with the MIT-Germany Seed Fund "Global Water Cycle and Environmental Monitoring using Active and Passive Satellite-based Microwave Instruments".

REFERENCES

- P. Marzahn and R. Ludwig, "On the derivation of soil surface roughness from multi parametric PolSAR data and its potential for hydrological modeling," in *Hydrol. Earth Syst. Sci.*, 13, 381-394, 2009, DOI: 10.5194/hess-13-381-2009.
- P. K. Srivastava, P. O'Neill, M. Cosh, M. Kurum, R. Lang and A. Joseph, "Evaluation of Dielectric Mixing Models for Passive Microwave Soil Moisture Retrieval Using Data From ComRAD Ground-Based SMAP Simulator," in *IEEE Journal of Selected Topics in Applied Earth Observations and Remote Sensing*, vol. 8, no. 9, pp. 4345-4354, Sept. 2015, DOI: 10.1109/JSTARS.2014.2372031.
 D. Entekhabi *et al.*, "The Soil Moisture Active Passive (SMAP)
- [3] D. Entekhabi et al., "The Soil Moisture Active Passive (SMAP) Mission," in *Proceedings of the IEEE*, vol. 98, no. 5, pp. 704-716, May 2010, DOI: 10.1109/JPROC.2010.2043918.
- [4] B. J. Choudhury, T. J. Schmugge, A. Chang and R. W. Newton, "Effect of surface roughness on the microwave emission from soils," in *J. Geophys. Res.*, 84(C9), 5699–5706, 1979, DOI: 10.1029/JC084iC09p05699.

- [5] P. Marzahn, D. Rieke-Zapp, and R. Ludwig, "Assessment of soil surface roughness statistics for microwave remote sensing applications using a simple photogrammetric acquisition system," in *ISPRS Journal* of Photogrammetry and Remote Sensing, vol. 72, pp. 80-89, 2012, DOI: 10.1016/j.isprsjprs.2012.06.005.
- [6] D. Rieke-Zapp, H. Wegmann, F. Santel, M.A. Nearing, "Digital photogrammetry for measuring soil surface roughness," in 2001 Proceedings of the American Society of Photogrammetry & Remote Sensing. Presented at Gateway to the New Millennium. St. Louis, Missouri, USA. 23.-27.04.2001.
- [7] E. G. Njoku et al., "Observations of soil moisture using a passive and active low-frequency microwave airborne sensor during SGP99," in *IEEE Transactions on Geoscience and Remote Sensing*, vol. 40, no. 12, pp. 2659-2673, Dec. 2002, DOI: 10.1109/TGRS.2002.807008.
- [8] F.T. Ulaby, D.G. Long, W. Blackwell, Ch. Elachi, A. Fung, C. Ruf, K. Sarabandi, H. Zebker and J.J. van Zyl, Microwave radar and radiometric remote sensing. University of Michigan. Press Ann Arbor, 2014.
- [9] P. S. Narvekar, D. Entekhabi, S. Kim and E. G. Njoku, "Soil Moisture Retrieval Using L-Band Radar Observations," in *IEEE Transactions on Geoscience and Remote Sensing*, vol. 53, no. 6, pp. 3492-3506, June 2015, DOI: 10.1109/TGRS.2014.2377714.
- [10] N. N. Das, D. Entekhabi and E. G. Njoku, "An Algorithm for Merging SMAP Radiometer and Radar Data for High-Resolution Soil-Moisture Retrieval," in *IEEE Transactions on Geoscience and Remote Sensing*, vol. 49, no. 5, pp. 1504-1512, May 2011, DOI: 10.1109/TGRS.2010.2089526.
- [11] J., Shi, J., Wang, A. Y. Hsu, P. E. O'Neill and E. T. Engman, "Estimation of bare surface soil moisture and surface roughness parameter using L-band SAR image data," in *IEEE Transactions on Geoscience and Remote Sensing*, vol. 35, no. 5, pp. 1254-1266, Sept. 1997, DOI: 10.1109/36.628792.
- [12] Y. Oh, K. Sarabandi and F. T. Ulaby, "An empirical model and an inversion technique for radar scattering from bare soil surfaces," in *IEEE Transactions on Geoscience and Remote Sensing*, vol. 30, no. 2, pp. 370-381, March 1992, DOI: 10.1109/36.134086.
- [13] M. C. Dobson and F. T. Ulaby, "Preliminaly Evaluation of the SIR-B Response to Soil Moisture, Surface Roughness, and Crop Canopy Cover," in *IEEE Transactions on Geoscience and Remote Sensing*, vol. GE-24, no. 4, pp. 517-526, July 1986, DOI: 10.1109/TGRS.1986.289666.
- [14] J. Kolassa, R.H. Reichle, C.S. Draper, "Merging active and passive microwave observations in soil moisture data assimilation", in *Remote Sensing of Environment*, vol. 191, pp. 117-130, 2017, DOI: 10.1016/j.rse.2017.01.015.
- [15] E. Santi, S. Paloscia, S. Pettinato, G. Fontanelli, "Application of artificial neural networks for the soil moisture retrieval from active and passive microwave spaceborne sensors", in *International Journal of Applied Earth Observation and Geoinformation*, vol. 48, pp. 61-73, 2016, DOI: 10.1016/j.jag.2015.08.002.
- [16] U. Narayan, V. Lakshmi and E. Njoku, "Retrieval of Soil Moisture from Passive and Active L/S Band Sensor (PALS) Observations During the Soil Moisture Experiment in 2002 (SMEX02)," in *Remote Sens. Env.*, 92, 483-496, 2004, DOI: 10.1016/j.rse.2004.05.018.
- [17] M. Piles, D. Entekhabi and A. Camps, "A Change Detection Algorithm for Retrieving High-Resolution Soil Moisture From SMAP Radar and Radiometer Observations," in *IEEE Transactions on Geoscience and Remote Sensing*, vol. 47, no. 12, pp. 4125-4131, Dec. 2009, DOI: 10.1109/TGRS.2009.2022088.
- [18] J. D. Ouellette et al., "A Time-Series Approach to Estimating Soil Moisture From Vegetated Surfaces Using L-Band Radar Backscatter," in *IEEE Transactions on Geoscience and Remote Sensing*, vol. 55, no. 6, pp. 3186-3193, June 2017.
- [19] N. N. Das, D. Entekhabi, E. G. Njoku, J. J. C. Shi, J. T. Johnson and A. Colliander, "Tests of the SMAP Combined Radar and Radiometer Algorithm Using Airborne Field Campaign Observations and Simulated Data," in *IEEE Transactions on Geoscience and Remote Sensing*, vol. 52, no. 4, pp. 2018-2028, April 2014, DOI: 10.1109/TGRS.2013.2257605.
- [20] D. Entekhabi, N. N. Das, E.G. Njoku, S. Yueh, J.T. Johnson and J. Shi, Soil Moisture Active Passive (SMAP). Algorithm Theoretical Basis Document L2 & L3 Radar/Radiometer Soil Moisture (Active/Passive) Data Products. Revision A. Jet Propulsion Lab., California Inst. Technol., Pasadena, CA, USA, 2014.

- [21] S. Saatchi, E. Njoku, U. Wegmuller, "Synergism of active and passive microwave data for estimating bare soil surface moisture", in ESA/NASA Int. Workshop Passive Microwave Remote Sens. Res. Related to Land-atmosphere. Interactions, Saint-Lary, France, Jan. 11-15 1993, pp. 205-224.
- [22] F. T. Ulaby, R. K. Moore and A. K. Fung, Microwave remote sensing: Active and passive. Volume 2-Radar remote sensing and surface scattering and emission theory. Boston, USA, Artech House, 1982.
- [23] J.-P. Wigneron, Y. Kerr, P. Waldteufel, K. Saleh, M.-J. Escorihuela, P. Richaume, P. Ferrazzoli, P. de Rosnay, R. Gurney, J.-C. Calvet, J.P. Grant, M. Guglielmetti, B. Hornbuckle, C. Mätzler, T. Pellarin and M. Schwank, "L-band Microwave Emission of the Biosphere (L-MEB) Model: Description and calibration against experimental data sets over crop fields," in *Remote Sensing of Environment*, vol. 107, issue 4, pp. 639-655, 2007, DOI: 10.1016/j.rse.2006.10.014.
- [24] J.-P. Wigneron, T.J. Jackson, P. O'Neill, G. De Lannoy, P. de Rosnay, J.P. Walker, P. Ferrazzoli, V. Mironov, S. Bircher, J.P. Grant, M. Kurum, M. Schwank, J. Munoz-Sabater, N. Das, A. Royer, A. Al-Yaari, A. Al Bitar, R. Fernandez-Moran, H. Lawrence, A. Mialon, M. Parrens, P. Richaume, S. Delwart and Y. Kerr, "Modelling the passive microwave signature from land surfaces: A review of recent results and application to the L-band SMOS & SMAP soil moisture retrieval algorithms," in *Remote Sensing of Environment*, vol. 192, pp. 238-262, 2017, DOI: 10.1016/j.rse.2017.01.024.
- [25] N.E. Verhoest, H. Lievens, W. Wagner, J. Álvarez-Mozos, M.S. Moran, F. Mattia, "On the Soil Roughness Parameterization Problem in Soil Moisture Retrieval of Bare Surfaces from Synthetic Aperture Radar," in *Sensors*, vol. 8, pp. 4213-4248, 2008, DOI: 10.3390/s8074213.
- [26] U. Wegmuller and C. Matzler, "Rough bare soil reflectivity model," in IEEE Transactions on Geoscience and Remote Sensing, vol. 37, no. 3, pp. 1391-1395, May 1999, DOI: 10.1109/36.763303.
- [27] T. Mo, B.J. Choudhury, T.J. Schmugge, J.R. Wang and T.J. Jackson, "A Model for Microwave Emission from Vegetation-Covered Soils," in *Journal of Geophysical Research*, vol. 87, pp. 229-237, 1982, DOI: 10.1029/JC087iC13p11229.
- [28] J. R. Wang, and B. J. Choudhury, "Remote sensing of soil moisture content over bare field at 1.4 GHz frequency," in *J. Geophys. Res.*, 86(C6), 5277–5282, 1981, DOI: 10.1029/JC086iC06p05277.
- [29] H. Lawrence, J. Wigneron, F. Demontoux, A. Mialon and Y. H. Kerr, "Evaluating the Semiempirical H - Q Model Used to Calculate the L-Band Emissivity of a Rough Bare Soil," in *IEEE Transactions on Geoscience and Remote Sensing*, vol. 51, no. 7, pp. 4075-4084, July 2013, DOI: 10.1109/TGRS.2012.2226995.
- [30] T. Mo and T. J. Schmugge, "A Parameterization of the Effect of Surface Roughness on Microwave Emission," in *IEEE Transactions on Geoscience and Remote Sensing*, vol. GE-25, no. 4, pp. 481-486, July 1987, DOI: 10.1109/TGRS.1987.289860.
- [31] W. Dierking, "RMS slope of exponentially correlated surface roughness for radar applications," in *IEEE Transactions on Geoscience* and Remote Sensing, vol. 38, no. 3, pp. 1451-1454, May 2000, DOI: 10.1109/36.843040.
- [32] Fung, A.K. Microwave scattering and emission models and their applications; Artech House: Boston, MA, 1994.
- [33] D. Entekhabi, S. Yueh, P. O'Neill, K.H. Kellogg and E. Al, SMAP Handbook, 2014.
- [34] R. Akbar, M. H. Cosh, P. E. O'Neill, D. Entekhabi and M. Moghaddam, "Combined Radar–Radiometer Surface Soil Moisture and Roughness Estimation," in *IEEE Transactions on Geoscience and Remote Sensing*, vol. 55, no. 7, pp. 4098-4110, July 2017, DOI: 10.1109/TGRS.2017.2688403.
- [35] SMAP data 2015 (NASA). Dataset: SMAP_L1B_S0_LoRes_V2. Retrieved from ASF DAAC 7 December 2015. DOI: 10.5067/J4SZZV52B88J.
- [36] S. Chan, E.G. Njoku and A. Colliander, SMAP L1C Radiometer Halforbit 36 km EASE-grid Brightness Temperatures, Version 3. Global Projection. NASA National Snow and Ice Data Center Distributed Active Archive Center, Boulder, Colorado USA, 2016, DOI: 10.5067/E51BSP6V3KP7. [08/30/2017].
- [37] P.E. O'Neill et al., SMAP L3 Radiometer Global Daily 36 km EASE-Grid Soil Moisture, Version 4. Global Projection. NASA National Snow and Ice Data Center Distributed Active Archive Center, Boulder, Colorado USA, 2016, DOI: 10.5067/OBBHQ5W22HME. [08/30/2017].

- [38] A.G. Konings, M. Piles, N. N. Das and D. Entekhabi, "L-band vegetation optical depth and effective scattering albedo estimation from SMAP," in *Remote Sensing of Environment*, vol. 198, pp. 460-470, 2017, DOI: 10.1016/j.rse.2017.06.037.
- [39] X. Xu et al., SMAP L3 Radiometer Northern Hemisphere Daily 36 km EASE-Grid Freeze/Thaw State, Version 1. Global Projection. Boulder, Colorado USA. NASA National Snow and Ice Data Center Distributed Active Archive Center, 2016, DOI: 10.5067/RDEJQEETCNWV. [08/30/17].
- [40] C. Utku and D. M. Le Vine, "Topographic Signatures in Aquarius Radiometer and Scatterometer Response," in *IEEE Transactions on Geoscience and Remote Sensing*, vol. 52, no. 7, pp. 4141-4154, July 2014, DOI: 10.1109/TGRS.2013.2280015.
- [41] A. Monerris, P. Benedicto, M. Vall-llossera, A. Camps, E. Santanach, M. Piles, and R. Prehn, "Assessment of the topography impact on microwave radiometry at L-band," in *J. Geophys. Res.*, 113, B12202, 2008, DOI: 10.1029/2008JB005602.
- [42] A. Mialon, L. Coret, Y. H. Kerr, F. Secherre and J. Wigneron, "Flagging the Topographic Impact on the SMOS Signal," in *IEEE Transactions on Geoscience and Remote Sensing*, vol. 46, no. 3, pp. 689-694, March 2008, DOI: 10.1109/TGRS.2007.914788.
- [43] Jarvis A., H.I. Reuter, A. Nelson, E. Guevara, 2008, Hole-filled seamless SRTM data V4, International Centre for Tropical Agriculture (CIAT), available from http://srtm.csi.cgiar.org.
- [44] Jagdhuber, T. et al., "Physics-Based Modeling of Active and Passive Microwave Covariations Over Vegetated Surfaces," in *IEEE Transactions on Geoscience and Remote Sensing*, vol. 57, issue 2, pp. 788-802, 2018, DOI: 10.1109/TGRS.2018.2860630.
- [45] T. Jagdhuber et al., "Physically-based retrieval of SMAP active-passive measurements covariation and vegetation structure parameters," 2016 IEEE International Geoscience and Remote Sensing Symposium (IGARSS), Beijing, 2016, pp. 3078-3081, DOI: 10.1109/IGARSS.2016.7729796.
- [46] G.C., Topp, Davis, J.L.; Annan, A.P., "Electromagnetic determination of soil water content: Measurements in coaxial transmission lines," in Water Resour. Res., vol. 16, pp. 574–582, 1980, DOI:10.1029/WR016i003p00574.
- [47] K. S. Chen, Tzong-Dar Wu, Leung Tsang, Qin Li, Jiancheng Shi and A. K. Fung, "Emission of rough surfaces calculated by the integral equation method with comparison to three-dimensional moment method simulations," in *IEEE Transactions on Geoscience and Remote Sensing*, vol. 41, no. 1, pp. 90-101, Jan. 2003, DOI: 10.1109/TGRS.2002.807587.
- [48] A.K. Fung et al., "An Improved IEM Model for Bistatic Scattering From Rough Surfaces," in Journal of Electromagnetic Waves and Applications, 16, pp. 689–702, 2002. DOI: 10.1163/156939302X01119.
- [49] L. Tsang et al., "Active and Passive Vegetated Surface Models With Rough Surface Boundary Conditions From NMM3D," in IEEE Journal of Selected Topics in Applied Earth Observations and Remote Sensing, vol. 6, no. 3, pp. 1698-1709, June 2013, DOI: 10.1109/JSTARS.2013.2257694.
- [50] C.A. Mack, "Analytic form for the power spectral density in one, two, and three dimensions," in *J. Micro/Nanolith, MEMS MOEMS*, 10(4), Oct. 2011, DOI: 10.1117/1.3663567.
- [51] J.A. Ogilvy and J.R. Foster, "Rough surfaces: gaussian or exponential statistics?" in *J. Phys. D: Appl. Phys*, vol. 22, pp. 1243-1251, 1989, DOI: 10.1088/0022-3727/22/9/001.
- [52] Agricultural Institute, Bureau of Meteorology, Australian Government: http://www.bom.gov.au/climate/data/index.shtml?bookmark=136 [07/27/2018].
- [53] N.N. Das, Ancillary Data Report: Soil Attributes. Jet Propuls. Lab. Calif. Inst. Technol., JPL D-53058, 2013.
- [54] W.R. Wieder, J. Boehnert, G.B. Bonan, and M. Langseth, "Regridded Harmonized World Soil Database v1.2. Data set. Available online [http://daac.ornl.gov] from Oak Ridge National Laboratory Distributed Active Archive Center, Oak Ridge, Tennessee, USA", 2014, DOI: http://dx.doi.org/10.3334/ORNLDAAC/1247.
- [55] R. Bindlish, T. Jackson, R. Sun, M. Cosh, S. Yueh and S. Dinardo, "Combined Passive and Active Microwave Observations of Soil Moisture During CLASIC," in *IEEE Geoscience and Remote Sensing Letters*, vol. 6, no. 4, pp. 644-648, Oct. 2009, DOI: 10.1109/LGRS.2009.2028441.
- [56] D. M. Le Vine, G. S. E. Lagerloef, F. R. Colomb, S. H. Yueh and F. A. Pellerano, "Aquarius: An Instrument to Monitor Sea Surface Salinity

- From Space," in *IEEE Transactions on Geoscience and Remote Sensing*, vol. 45, no. 7, pp. 2040-2050, July 2007, DOI: 10.1109/TGRS.2007.898092.
- [57] V. Gupta and R. Jangid, "Microwave response of rough surfaces with autocorrelation functions, RMS heights and correlation lengths using active remote sensing," in *Indian Journal of Radio and Space Physics*, 40, pp. 137–146, 2011.
- [58] N. Baghdadi, M. Zribi, S. Paloscia, N. Verhoest, H. Lievens, F. Baup and F. Mattia, "Semi-Empirical Calibration of the Integral Equation Model for Co-Polarized L-Band Backscattering," in *Remote Sensing*, 7, pp. 13626–13640, 2015, DOI:10.3390/rs71013626.
- [59] J. Peng, A. Loew, O. Merlin and N.E.C. Verhoest, "A review of spatial downscaling of satellite remotely sensed soil moisture," in *Rev. Geophys.*, 55, pp. 1-26, 2017, DOI: 10.1002/2016RG000543.
- [60] L. Zhixiong, C. Nan, U.D. Perdok and W.B. Hoogmoed, "Characterisation of Soil Profile Roughness," in *Biosystems Engineering*, 91, pp. 369–377, 2005, DOI: 10.1016/j.biosystemseng.2005.04.004.
- [61] M. Kurum, P.E. O'Neill, R.H. Lang, A.T. Joseph, M.H. Cosh, T.J. Jackson, "Effective tree scattering and opacity at L-band," in *Remote Sensing of Environment*, vol. 118, pp. 1-9, 2012, DOI: 10.1016/j.rse.2011.10.024.
- [62] L. Zhao, X. Liang, & F. Wu, "Soil surface roughness change and its effect on runoff and erosion on the Loess Plateau of China," in J. Arid Land 6, pp. 400–409, 2014, DOI: 10.1007/s40333-013-0246-z.
- [63] A. Fluhrer et al., "Physics-Based Retrieval of Surface Roughness Parameters for Bare Soils from Combined Active-Passive Microwave Signatures," IGARSS 2018 - 2018 IEEE International Geoscience and Remote Sensing Symposium, Valencia, 2018, pp. 337-340, DOI: 10.1109/IGARSS.2018.8519563.
- [64] D. van der Wal, P. M. J. Herman and A. Wielemaker-van den Dool, "Characterisation of surface roughness and sediment texture of intertidal flats using ERS SAR imagery," in *Remote Sensing of Environment*, vol. 98, issue 1, pp. 96-109, 2005, DOI: 10.1016/j.rse.2005.06.004.



Anke Fluhrer (S'17–M'18) received the B.S. degree in geography from the Julius-Maximilians-University Würzburg, Würzburg, Germany, in 2014, and the M.S. degree in physical geography from the Friedrich-Alexander University Erlangen-Nuremberg, Erlangen, Germany, in 2018. She is currently a Research Associate with the prospect of a Ph.D. at the Microwaves and Radar Institute (HR) of the German Aerospace Center (DLR), Oberpfaffenhofen, Germany. Her research interests include terrestrial

remote sensing, satellite image processing, and data assimilation.



Thomas Jagdhuber (S'08–M'12–SM'19) received his Diploma degree (with honors) in physical geography, physics, remote sensing and geoinformatics from Ludwig Maximilian University of Munich, Munich, Germany, in 2006 and his PhD degree (with honors) in hydrology from the Faculty of Science at the University of Potsdam, Potsdam, Germany, in 2012. His main research interests include physics-based multi-sensor data integration with focus on active and passive microwave interaction theory

and on polarimetric techniques for hydrological, cryosphere and agricultural parameter modeling and estimation. Since 2007 he is affiliated with the Microwaves and Radar Institute (HR) of the German Aerospace Center (DLR). In 2014 he was honored with the DLR Science Award for his research on polarimetric SAR decomposition techniques. From 2014 through 2019, he was a yearly visiting scientist at the Massachusetts Institute of Technology (MIT), Boston, USA, contributing to the preparation and continuation of the SMAP and SMAP/Sentinel-1 missions. Together with Prof. Dr. Entekhabi (MIT), he was awarded with the MIT-MISTI grant for global water cycle and environmental monitoring using active and passive satellite-based microwave instruments. In addition, Dr. Jagdhuber serves as a lecturer for the University of Jena and the University of Augsburg as well as a reviewer for several international journals and conference boards.



Ruzbeh Akbar (S'05–M'13) received the B.S. (summa cum laude) degree from The George Washington University, Washington, DC, USA, in 2009, the M.S. degree from the University of Michigan, Ann Arbor, MI, USA, in 2011, and the Ph.D. degree from the University of Southern California, Los Angeles, CA, USA, in 2016, all in electrical engineering. He is currently a Postdoctoral Research Associate with the Massachusetts Institute of Technology, Cambridge, MA, USA. His research interests include terrestrial remote sensing,

electromagnetic theory, and hydrology. Dr. Akbar was a recipient of the NASA Earth and Space Science Fellowship from 2010 to 2014.



Peggy E. O'Neill (F'16) received the B.S. (summa cum laude) degree (Hons.) in geography from Northern Illinois University, DeKalb, IL, USA, in 1976, and the M.A. degree in geography from the University of California at Santa Barbara, Santa Barbara, CA, USA, in 1979. She has done postgraduate research in civil and environmental engineering at Cornell University, Ithaca, NY, USA. Since 1980, she has been a Physical Scientist with the Hydrological Sciences Laboratory, NASA/Goddard

Space Flight Center, Greenbelt, MD, USA, where she conducts research in soil moisture retrieval and land surface hydrology, primarily through microwave remote sensing techniques. She is currently the SMAP Deputy Project Scientist.



Dara Entekhabi (M'04, SM'09, Fellow'15) received B.S. (1983) and M.S. degrees (1985, 1988) in geography from Clark University, Worcester, MA and Ph.D. degree (1990) in civil and environmental engineering from the Massachusetts Institute of Technology (MIT), Cambridge, MA. He is currently a Professor with the Department of Civil and Environmental Engineering and the Department of Earth, Atmospheric and Planetary Sciences, MIT. He is the Science Team lead for the National Aeronautics and Space Administration's Soil Moisture Active and

Passive (SMAP) mission that was launched January 31, 2015. His research includes terrestrial remote sensing, data assimilation, and coupled land–atmosphere systems modeling. Prof. Entekhabi is also a Fellow of the American Meteorological Society and the American Geophysical Union. He is a member of the National Academy of Engineering.